

Tunable superconducting resonators via on-chip control of local magnetic field

Chen-Guang Wang, Wen-Cheng Yue, Xuecou Tu, Tianyuan Chi, Tingting Guo, Yang-Yang Lyu, Sining Dong, Chunhai Cao, Labao Zhang, Xiaoqing Jia, Guozhu Sun, Lin Kang, Jian Chen, Yong-Lei Wang, Huabing Wang, and Peiheng Wu

Citation: Chin. Phys. B, 2024, 33 (**5**): 058402. DOI: 10.1088/1674-1056/ad2f21
Journal homepage: http://cpb.iphy.ac.cn; http://iopscience.iop.org/cpb

What follows is a list of articles you may be interested in

Switchable and tunable triple-channel bandpass filter

Ming-En Tian(田明恩), Zhi-He Long(龙之河), Li-Jun Feng(冯丽君), Lei-Lei He(贺磊磊), and Tian-Liang Zhang(张天良)
Chin. Phys. B, 2022, 31 (**7**): 078401. DOI: 10.1088/1674-1056/ac4f4f

A high rectification efficiency $Si_{0.14}Ge_{0.72}Sn_{0.14}$–$Ge_{0.82}Sn_{0.18}$–Ge quantum structure n-MOSFET for 2.45 GHz weak energy microwave wireless energy transmission

Dong Zhang(张栋), Jianjun Song(宋建军), Xiaohuan Xue(薛笑欢), and Shiqi Zhang(张士琦)
Chin. Phys. B, 2022, 31 (**6**): 068401. DOI: 10.1088/1674-1056/ac339e

Integrated superconducting circuit for qubit and resonator protection

Xiao-Pei Yang(杨晓沛), Zhi-Kun Han(韩志坤), Shu-Qing Song(宋树清), Wen Zheng(郑文), Dong Lan(兰栋), Xin-Sheng Tan(谭新生), and Yang Yu(于扬)
Chin. Phys. B, 2021, 30 (**7**): 078403. DOI: 10.1088/1674-1056/ac003d

Compact NbN resonators with high kinetic inductance

Xing-Yu Wei(魏兴雨), Jia-Zheng Pan(潘佳政), Ya-Peng Lu(卢亚鹏), Jun-Liang Jiang(江俊良), Zi-Shuo Li(李子硕), Sheng Lu(卢盛), Xue-Cou Tu(涂学凑), Qing-Yuan Zhao(赵清源), Xiao-Qing Jia(贾小氢), Lin Kang(康琳), Jian Chen(陈健), Chun-Hai Cao(曹春海), Hua-Bing Wang(王华兵), Wei-Wei Xu(许伟伟), Guo-Zhu Sun(孙国柱), and Pei-Heng Wu(吴培亨)
Chin. Phys. B, 2020, 29 (**12**): 128401. DOI: 10.1088/1674-1056/abc2b8

The coupling effect of air-bridges on broadband spiral inductors in SiC-based MMIC technology

Jia-Xin Zheng(郑佳欣), Xiao-Hua Ma(马晓华), Yang Lu(卢阳), Bo-Chao Zhao(赵博超), Heng-Shuang Zhang(张恒爽), Meng Zhang(张濛), Li-Xiang Chen(陈丽香), Qing Zhu(朱青), Yue Hao(郝跃)
Chin. Phys. B, 2017, 26 (**8**): 088401. DOI: 10.1088/1674-1056/26/8/088401

Tunable superconducting resonators via on-chip control of local magnetic field

Chen-Guang Wang(王晨光)[1,2], Wen-Cheng Yue(岳文诚)[1], Xuecou Tu(涂学凑)[1], Tianyuan Chi(迟天圆)[1], Tingting Guo(郭婷婷)[1], Yang-Yang Lyu(吕阳阳)[1], Sining Dong(董思宁)[1,3], Chunhai Cao(曹春海)[1], Labao Zhang(张蜡宝)[1,4], Xiaoqing Jia(贾小氢)[1,4], Guozhu Sun(孙国柱)[1,4], Lin Kang(康琳)[1,4], Jian Chen(陈健)[1,2], Yong-Lei Wang(王永磊)[1,2,3,†], Huabing Wang(王华兵)[1,2,‡], and Peiheng Wu(吴培亨)[1,2]

[1] *Research Institute of Superconductor Electronics, School of Electronic Science and Engineering, Nanjing University, Nanjing* 210023, *China*
[2] *Purple Mountain Laboratories, Nanjing* 211111, *China*
[3] *National Key Laboratory of Spintronics, Nanjing University, Suzhou* 215163, *China*
[4] *Hefei National Laboratory, Hefei* 230094, *China*

(Received 22 February 2024; revised manuscript received 26 February 2024; accepted manuscript online 1 March 2024)

Superconducting microwave resonators play a pivotal role in superconducting quantum circuits. The ability to fine-tune their resonant frequencies provides enhanced control and flexibility. Here, we introduce a frequency-tunable superconducting coplanar waveguide resonator. By applying electrical currents through specifically designed ground wires, we achieve the generation and control of a localized magnetic field on the central line of the resonator, enabling continuous tuning of its resonant frequency. We demonstrate a frequency tuning range of 54.85 MHz in a 6.21-GHz resonator. This integrated and tunable resonator holds great potential as a dynamically tunable filter and as a key component of communication buses and memory elements in superconducting quantum computing.

Keywords: superconducting resonator, NbN, kinetic inductance, tunable resonator

PACS: 84.40.Dc, 85.25.Am **DOI:** 10.1088/1674-1056/ad2f21

1. Introduction

Superconducting microwave resonators are key elements in applications such as photon detection[1] and quantum computing,[2] owing to their simplicity in fabrication, ease of integration, and low energy loss. The demand for superconducting resonators with *in-situ* tunable resonance frequencies has grown across diverse applications, including parametric amplifiers,[3–6] spectrometers,[7] magnetometers,[8] and microwave storage devices.[9] The frequency tunability can be achieved by tuning the nonlinear inductance of a superconducting quantum interference device (SQUID).[3,10–12] While these SQUID-based resonators usually exhibit substantial frequency tuning range due to the considerable nonlinear inductance of Josephson junctions, the relatively low critical currents of Josephson junctions prevent their applications with high operating power[6] or in strong magnetic fields.[13] In contrast, the resonant frequency of superconducting resonators can be tuned by altering the kinetic inductance of superconductors.[13–19] This can be achieved by injecting a DC current into the resonator from an integrated DC bias circuit.[14–16] However, this unavoidably introduces additional losses to resonators. This limitation can be overcome by tuning the kinetic inductance of superconductors using magnetic fields, leading to remote tuning of superconducting resonators without the need for adding additional circuits into the resonator line.[13,17–19] However, in all previously demonstrated magnetic field-tunable superconducting resonators, the magnetic field is applied externally to the entire chip. This not only hinders applications in magnetic field-sensitive systems[20–24] but also limits their potential for large-scale integration. In this work, we address these limitations with a unique approach, on-chip generating a local magnetic field to control the resonance frequency of a superconducting coplanar waveguide (CPW) resonator. This is achieved by applying anti-parallel supercurrents through two meticulously designed ground lines, which effectively confines the magnetic field to the resonator's central line, thus presenting notable advantage for system integration.

2. Device fabrication and parameters

The kinetic inductance of a superconductor is proportional to the superconducting penetration depth.[25] Niobium nitride (NbN) is known for its long penetration depth, ranging from 300 nm to 400 nm.[26] Thus, in this study, we utilize NbN films to fabricate the superconducting resonator. As illustrated in Fig. 1, our device consists of a half-wavelength CPW resonator capacitively coupled to a feedline. First, a 22-nm thick NbN film is sputtered onto a C-plane sapphire substrate, and then the device structure is formed using standard

†Corresponding author. E-mail: yongleiwang@nju.edu.cn
‡Corresponding author. E-mail: hbwang@nju.edu.cn

© 2024 Chinese Physical Society and IOP Publishing Ltd

photolithography followed by CF_4 dry etching. Two current ground lines are separated from the ground plane, each with one side directly connected to the ground plane and the other side linked to DC sources. To transmit higher supercurrent through the ground wires for generating higher magnetic field, we increase the thickness of the two ground wires with 270-nm thick NbN film, achieved through the standard photolithography and lift-off techniques. Because magnetic field produces superconducting vortices, the quantized magnetic fluxes, in the center conductor, to avoid the vortices' motion induced energy losses, we introduce holes in the center conductor to pin the vortices.[27–30] This also generates circulating supercurrents around the holes when magnetic field is applied, thus altering the kinetic inductance of the center line.[17]

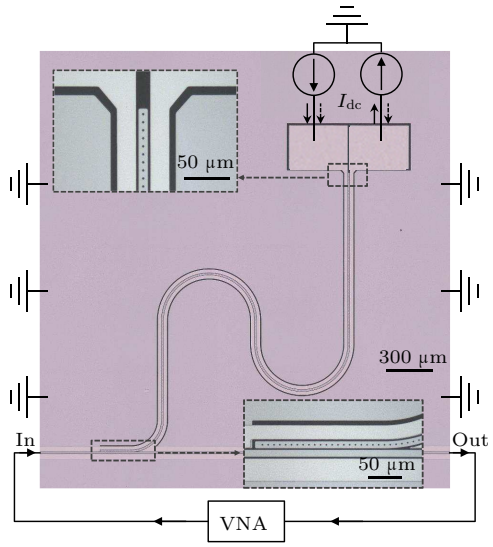


Fig. 1. Optical photography of the CPW resonator coupled to a feedline. The width and length of the resonator are 10 μm and 4289 μm, respectively. The diameter of the holes in the center conductor is approximately 3 μm. The length of the coupler between the resonator and the feedline is 200 μm.

The geometric inductance L_g and the capacitor C of the resonator can be calculated using conformal mapping.[31] They are given by

$$L_g = l \cdot \frac{\mu_0}{4} \frac{\mathrm{K}(k_0')}{\mathrm{K}(k_0)}, \tag{1}$$

$$C = l \cdot 4\varepsilon_0 \varepsilon_{\mathrm{eff}} \frac{\mathrm{K}(k_0')}{\mathrm{K}(k_0)}, \tag{2}$$

where l (≈ 4.3 mm) is the length of the CPW resonator, and $\varepsilon_{\mathrm{eff}}$ (≈ 6.3) is the effective permittivity of the CPW line. Here, K denotes the complete elliptic integral of the first kind with the arguments

$$k_0 = \frac{w}{w+2s}, \tag{3}$$

$$k_0' = \sqrt{1-k_0^2}, \tag{4}$$

where w is the width of the center conductor (10 μm), s is the gap between the center conductor and the ground wires (3 μm). Hence, the geometric inductance L_g is 1.509 nH, and the capacitor C is 0.854 pF. The fundamental mode f_0 of a half-wavelength resonator is given by $f_0 = 1/2\sqrt{(L_g + L_{k0})C}$, where L_{k0} denotes kinetic inductance.[31] The experimentally determined f_0 is around 6.21 GHz. Thus, we can determine the kinetic inductance $L_{k0} = 6.079$ nH.

Our device exhibits a high kinetic inductance ratio $\alpha = L_{k0}/(L_g + L_{k0}) \approx 0.801$, which is advantageous for tuning the resonant frequency by changing the kinetic inductance. The kinetic inductance can be tuned by magnetic field. The relation between the kinetic inductance of a superconductor and the magnetic field H is given by[2,19]

$$L_k(H) \approx L_{k0}\left(1 + \frac{H^2}{H_*^2}\right), \tag{5}$$

where L_{k0} is the kinetic inductance in zero magnetic field, and H_* is characteristic magnetic field related to critical magnetic field. L_k typically exhibits limited tunability due to $H \ll H_*$.[2] The resonance frequency shift ratio is given by

$$\frac{\Delta f}{f_0} = -\beta H^2, \tag{6}$$

where $\beta = \alpha/2H_*^2$. Hence, the frequency can be quadratically tuned by the applied magnetic field.

3. Local magnetic field generation

To generate a local magnetic field, a DC current is applied to the two ground lines, as illustrated in the schematic diagram in Fig. 2(a). Here, we investigate the effects of parallel and antiparallel currents flowing through the ground wires, respectively. When antiparallel currents flow through the ground wires, a magnetic field is locally generated on the center conductor of the resonator (Fig. 2(b)). In contrast, the magnetic fields generated by parallel currents in the two ground wires neutralize each other at the center conductor, as depicted in Fig. 2(c). The magnetic field can be calculated using Biot–Savart law. For an NbN film with a thickness of 22 nm, only the perpendicular component of the magnetic field (H_z, in the $Z = 0$ plane) contributes to the frequency tuning[19] and is given by

$$H_z = \frac{I_{dc}}{4\pi b}\left[\ln\frac{(y-a)^2}{(y-a-b)^2} \pm \ln\frac{(y+a)^2}{(y+a+b)^2}\right], \tag{7}$$

where I_{dc} is the current flowing through the ground wires. The "+" sign represents antiparallel currents, and the '−' sign denotes parallel currents.

In our experiment, applying a maximum antiparallel current of $I_{dc} = 100$ mA results in a 2.5-mT magnetic field at the center conductor (Fig. 2(d)). At a distance of 50 μm from the center conductor, the magnetic field decreases to 0.35 mT (Fig. 2(d)). The magnetic field weakens rapidly with increasing distance from the center conductor. This approach ensures that the locally generated magnetic field has a neglectable impact on other components integrated into the circuits.

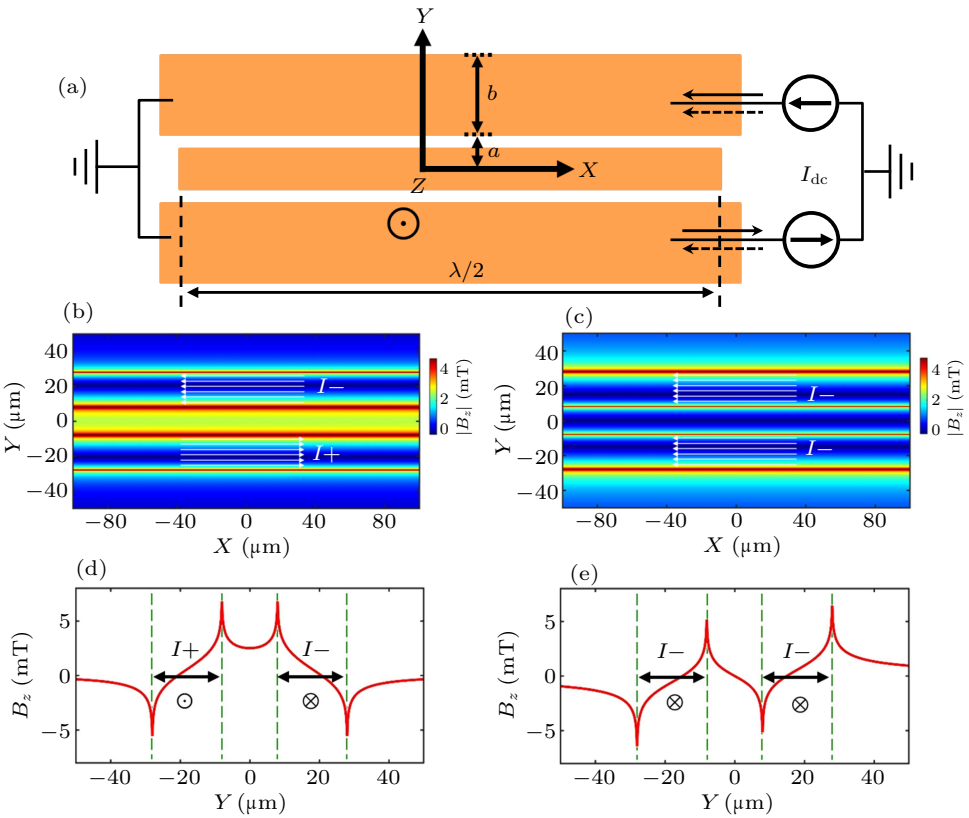


Fig. 2. (a) Schematic diagram of the resonator with current applied to the two ground lines. (b)–(c) Calculated magnetic field distribution on the resonator when applying antiparallel currents (b) and parallel currents (c). (d)–(e) Magnetic field distribution across the CPW resonator under antiparallel currents (d) and parallel currents (e).

4. Experimental results and analyses

To characterize the frequency tunability of our resonator, we recorded the forward transmission (S_{21}) using a vector network analyzer (VNA) at various ground line currents. The superconducting resonator was mounted in a dilution refrigerator operating at 20 mK. The input signal from the VNA was attenuated (−50 dB) to minimize the noise. The output signal, isolated by an isolator, was connected to the VNA through a high electron-mobility transistor amplifier with a gain of +42 dB. The on-chip input power is −70 dBm. First, we measured S_{21} at 20 mK while appling antiparallel currents (0 mA–100 mA) to the ground wires. As shown in Fig. 3(a), the resonance frequency of the resonator was suppressed with increasing currents, revealing a maximum frequency shift of 54.85 MHz from a 6.21-GHz resonance tone under $I_{dc} = 100$ mA.

Although the ground wires are superconducting, the contact resistance between bonding wires and electrodes could induce Joule heating when a significant current is applied. To examine the possible thermal effects on the frequency tuning, we compared the above results to measurements under a parallel-current configuration (Fig. 3(b)) as well as to those obtained by directly varying the temperature (Fig. 3(c)). As shown in Fig. 3(b), the resonance frequency remains relatively stable at low parallel currents, with a sudden shift observed beyond a certain current value ($\geq$ 80 mA). This is in contrast to the effects from antiparallel currents configuration, in which the resonance frequency gradually shifts with currents. Moreover, the frequency shift in the antiparallel-current configuration is much larger than that in the parallel-current configuration. Despite the Joule heating effect being equivalent between the antiparallel and parallel currents, the significantly larger frequency shift in the antiparallel-current configuration suggests that the observed frequency tuning in Fig. 3(a) is dominated by the local magnetic field produced from antiparallel currents in the ground wires.

On the other hand, as depicted in Fig. 3(c), the direct temperature-dependent results reveal a rapid weakening of the resonance signal strength, with a substantial shift (328 MHz) in resonance frequency as the temperature increases from 20 mK to 5 K. When comparing the effect of the antiparallel current configuration (Fig. 3(a)) to the temperature effect (Fig. 3(c)), it is evident that the resonance signal strength from the temperature effect is about 10 dB lower than that from the antiparallel current configuration for a similar frequency shift, as displayed by the dashed lines in Figs. 3(a) and 3(c). This further highlights the advancement of tuning resonance frequency using local magnetic field.

To quantitatively analyze our data, we employ the Diameter Correction Method (DCM)[32] to fit the S_{21} data and extract the resonant frequencies and quality factors. According to the

DCM model, the forward transmission can be expressed as

$$S_{21}(f) = 1 - \frac{Q_{\rm L}\,{\rm e}^{{\rm i}\phi}}{Q_{\rm e}} \frac{1}{1 + 2{\rm i}Q_{\rm L}\dfrac{f - f_0}{f_0}}, \tag{8}$$

where ϕ is the asymmetry factor of the resonator, f_0 is the resonance frequency, and $Q_{\rm L}$ is the loaded quality factor, defined as the parallel combination of internal ($Q_{\rm i}$) and external ($Q_{\rm e}$) quality factors:

$$\frac{1}{Q_{\rm L}} = \frac{1}{Q_{\rm e}} + \frac{1}{Q_{\rm i}}. \tag{9}$$

Figures 4(a) and 4(b) respectively display the experimental results (depicted by red lines in the figure) of the magnitude and the phase of the complex transmission data S_{21} obtained at 20 mK and with zero current in the ground lines. The corresponding fitting lines are shown in blue lines in Figs. 4(a) and 4(b). From the fittings, we obtain the internal quality factor $Q_{\rm i} \approx 8.2 \times 10^4$ and the zero-field resonant frequency $f_0 \approx 6.21$ GHz. The $Q_{\rm i}$ value is consistent with those reported previously for resonators fabricated from the same material,[33] revealing the high quality of our NbN film.

Figure 4(c) presents the extracted $I_{\rm dc}$-dependent frequency shift Δf for parallel-current (blue) and antiparallel-current (red) configurations. According to Eqs. (6) and (7), Δf induced by the magnetic field H is proportional to parameters H^2 and $I_{\rm dc}^2$. As depicted in the inset of Fig. 4(c), Δf for the antiparallel-current configuration changes linearly with $I_{\rm dc}^2$, in perfect agreement with the magnetic-field-induced resonance frequency shift mentioned earlier.

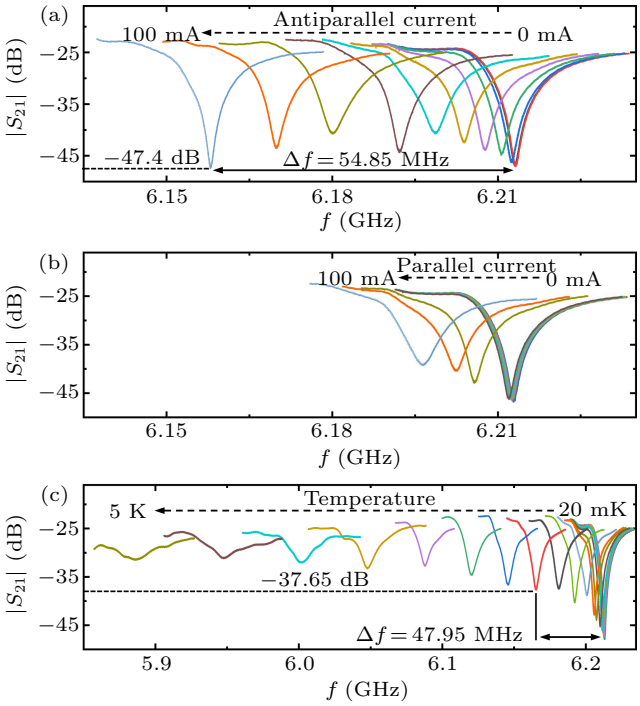


Fig. 3. The $|S_{21}|$ spectra of the tunable resonator. (a)–(b) Evolutions of $|S_{21}|$ spectra with antiparallel currents (a) and parallel currents (b), swept from 0 to 100 mA at 20 mK. (c) $|S_{21}|$ spectra as a function of temperature from 20 mK to 5 K.

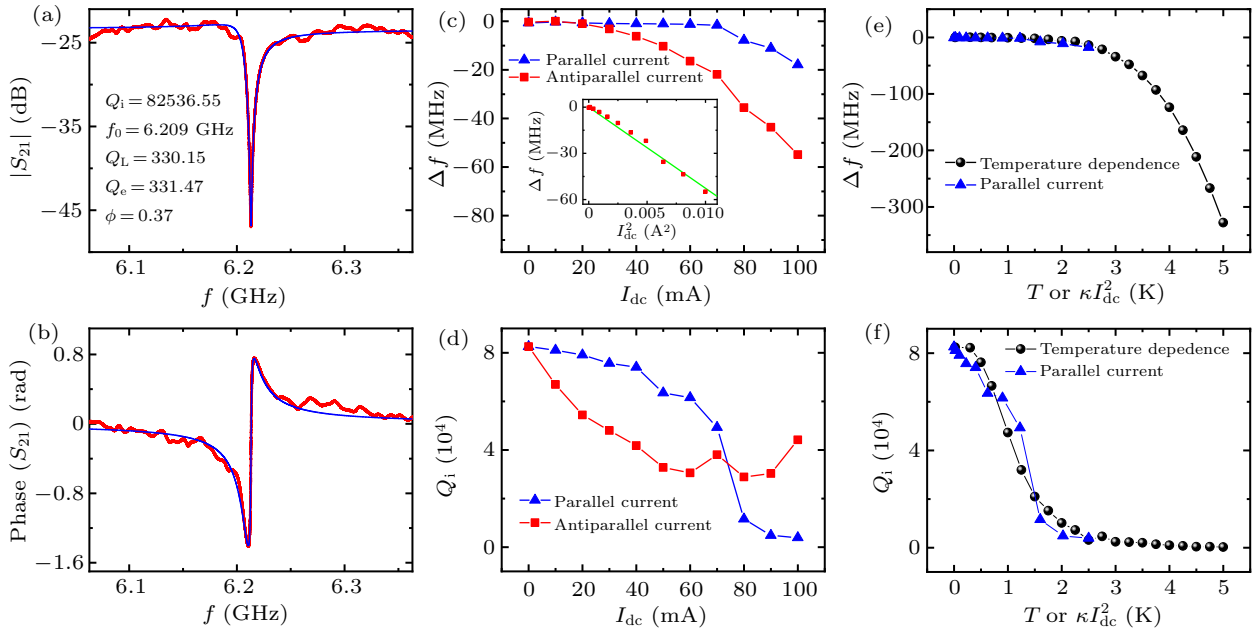


Fig. 4. Quantitative analysis of frequency tuning effects. (a)–(b) The resonance line shapes of experimental data (red) and fitting data (blue) for the magnitude (a) and phase (b) of S_{21}. (c)–(d) The frequency shift Δf (c) and the internal quality factor $Q_{\rm i}$ (d) as a function of parallel currents (blue) and antiparallel currents (red). The inset of panel (c) is the fitting of Δf to Eq. (6) for antiparallel-current configuration. (e) and (f) Comparison between parallel-current-dependent (blue) and temperature-dependent (black) frequency shift Δf (e) and the internal quality factor $Q_{\rm i}$ (f).

As indicated by the blue curve in Fig. 4(c), the Δf for the parallel-current configuration remains nearly zero until $I_{\rm dc} \geq 80$ mA. Beyond this point, the corresponding $Q_{\rm i}$ rapidly decreases and is lower than that for the antiparallel-current configuration (Fig. 4(d)). Notably, the $Q_{\rm i}$ (red curve in Fig. 4(d)) for the antiparallel-current configuration decreases very slowly for $I_{\rm dc} \geq 60$ mA, and in some instances, it may even slightly increase. This indicates a distinct role of the par-

allel currents compared to that of the antiparallel currents. In Figs. 4(e) and 4(f), we compare the evolutions of Δf and Q_i with parallel currents and those with the temperature. It can be seen that both Δf and Q_i curves can be perfectly normalized by $T = \kappa I_{dc}^2$, where T is temperature, and κ is a constant. This clearly indicates the frequency tuning in the parallel-current configuration is dominated by the Joule heating-induced temperate change. Figures 4(e) and 4(f) show that the effect of the applied maximal parallel current of $I_{dc} = 100$ mA corresponds to an effective temperature of 2.5 K.

Although one might anticipate equivalent Joule heating effects from parallel currents and antiparallel currents, the much larger and slightly increased Q_i with I_{dc} at $I_{dc} \geq 80$ mA (the red curve in Fig. 4(d)) indicates a negligible temperature-dependent effect for the antiparallel-current configuration compared to that for the parallel-current configuration. This suggests that parallel currents produce more dissipation than antiparallel currents. Two possible explanations for this effect are: (i) The parallel-current configuration requires current flowing through additional electrodes, thus resulting in larger Joule heating from contact resistance compared to that in the antiparallel-current configuration, as shown in Fig. S1. (ii) The parallel currents induce stronger effects on vortex motion in the ground lines, thus generating more dissipation than the antiparallel currents. The real mechanism behind the difference between parallel- and antiparallel-current configurations requires more detailed investigation in the future.

5. Conclusion and perspectives

In conclusion, our on-chip method of generating a local magnetic field by applying antiparallel currents to ground wires successfully achieves notable frequency tunability in superconducting resonators. The demonstrated superconducting resonator, featuring an internal quality factor of 8.2×10^4, a generated magnetic field of 2.5 mT, and a maximum frequency tunability of 54.85 MHz, holds substantial promise for the large-scale integration in quantum circuits. The confined local magnetic field, limited to the resonator's central line, ensures minimal impact on other integrated circuit components.

Our tunable superconducting resonators can benefit a range of applications, such as quantum computing[2–6,9–11] and single-photon detection.[1] The presence of ground lines that interrupt the ground plane lowers the internal quality factors in comparison to a standard CPW resonator (see Fig. S2). Improvements in grounding, either by reducing resistance or by increasing the capacitance between the ground lines and the external ground plane, could mitigate this issue. Further improving the frequency tuning performance could be possible by fine tuning the resonator's parameters, including materials, geometrical dimensions, and contact resistance. The unique behavior observed in experiments, wherein the frequency tuning effect is predominantly governed by the local magnetic field rather than thermal effects, emphasizes the effectiveness of our methodology. This investigation paves the way for further advancements in superconducting resonators for quantum technologies, highlighting the crucial role of on-chip local magnetic field control in the development of future integrated quantum systems.

Acknowledgements

Project supported by the National Key Research and Development Program of China (Grant Nos. 2021YFA0718802 and 2018YFA0209002), the National Natural Science Foundation of China (Grant Nos. 62274086, 62288101, 61971464, 62101243, and 11961141002), the Excellent Young Scholar Program of Jiangsu Province, China (Grant Nos. BK20200008 and BK20200060), the Outstanding Postdoctoral Program of Jiangsu Province, China, the Fundamental Research Funds for the Central Universities, and the Fund from Jiangsu Key Laboratory of Advanced Techniques for Manipulating Electromagnetic Waves.

References

[1] Day P K, LeDuc H G, Mazin B A, Vayonakis A and Zmuidzinas J 2003 *Nature* **425** 817
[2] Zmuidzinas J 2012 *Annu. Rev. Condens. Matter Phys.* **3** 169
[3] Castellanos-Beltrana M A and Lehnert K W 2007 *Appl. Phys. Lett.* **91** 083509
[4] Chaudhuri S, Li D, Irwin K D, Bockstiegel C, Hubmayr J, Ullom J N, Vissers M R and Gao J 2017 *Appl. Phys. Lett.* **110** 152601
[5] Tholén E A, Ergül A, Doherty E M, Weber F M, Grégis F and Haviland D B 2007 *Appl. Phys. Lett.* **90** 253509
[6] Eom1 B H, Day P K, LeDuc H G and Zmuidzinas J 2012 *Nat. Phys.* **8** 623
[7] Stoutimore M J A, Khalil M S, Lobb C J and Osborn K D 2012 *Appl. Phys. Lett.* **101** 062602
[8] Luomahaara J, Vesterinen V, Grönberg L and Hassel J 2014 *Nat. Commun.* **5** 4872
[9] Pierre M, Svensson I, Sathyamoorthy S R, Johansson G and Delsing P 2014 *Appl. Phys. Lett.* **104** 232604
[10] Wang Z L, Zhong Y P, He L J, Wang H, Martinis J M, Cleland A N and Xie Q W 2013 *Appl. Phys. Lett.* **102** 163503
[11] Palacios-Laloy A, Nguyen F, Mallet F, Bertet P, Vion D and Esteve D 2008 *J. Low Temp. Phys.* **151** 1034
[12] Strickland W M, Elfeky B H, Yuan J O, Schiela W F, Yu P, Langone D, Vavilov M G, Manucharyan V E and Shabani J 2023 *Phys. Rev. Appl.* **19** 034021
[13] Vissers M R, Hubmayr J, Sandberg M, Chaudhuri S, Bockstiegel C and Gao J 2015 *Appl. Phys. Lett.* **107** 062601
[14] Mahashabde S, Otto E, Montemurro D, Graaf S, Kubatkin S and Danilov A 2020 *Appl. Phys. Lett.* **14** 044040
[15] Adamyan A A, Kubatkin S E and Danilov A V 2016 *Appl. Phys. Lett.* **108** 172601
[16] Xu M, Han X, Fu W, Zou C L and Tang H X 2019 *Appl. Phys. Lett.* **114** 192601
[17] Zollitsch C W, O'Sullivan J, Kennedy O, Dold G and Morton J J L 2019 *AIP Adv.* **9** 125225
[18] Samkharadze N, Bruno A, Scarlino P, Zheng G, DiVincenzo D P, DiCarlo L and Vandersypen L M K 2016 *Phys. Rev. Appl.* **5** 044004
[19] Healey J E, Lindström T, Colclough M S, Muirhead C M and Tzalenchuk A Y 2008 *Appl. Phys. Lett.* **93** 043513
[20] Bienfait A, Campagne-Ibarcq P, Kiilerich A H, Zhou X, Probst S, Pla J J, Schenkel T, Vion D, Esteve D, Morton J J L, Moelmer K and Bertet P 2017 *Phys. Rev. X* **7** 041011

[21] Kroll J G, Borsoi F, Enden K L, Uilhoorn W, Jong D, Quintero-Pérez M, Woerkom D J, Bruno A, Plissard S R, Car D, Bakkers E P A M, Cassidy M C and Kouwenhoven L P 2019 *Phys. Rev. Appl.* **11** 064053
[22] Asfaw A T, Sigillito A J, Tyryshkin A M, Schenkel T and Lyon S A 2017 *Appl. Phys. Lett.* **111** 032601
[23] Grezes C, Julsgaard B, Kubo Y, Stern M, Umeda T, Isoya J, Sumiya H, Abe H, Onoda S, Ohshima T, Jacques V, Esteve J, Vion D, Esteve D, Mølmer K and Bertet P 2014 *Phys. Rev. X* **4** 021049
[24] Wesenberg J H, Ardavan A, Briggs G A D, Morton J J L, Schoelkopf R J, Schuster D I and Mølmer K 2009 *Phys. Rev. Lett.* **103** 070502
[25] Meservey R and Tedrow P M 1969 *J. Appl. Phys.* **40** 2028
[26] Kubo S, Asahi M, Hikita M and Igarashi M 1984 *Appl. Phys. Lett.* **44** 258
[27] Bothner D, Gaber T, Kemmler M, Koelle D and Kleiner R 2011 *Appl. Phys. Lett.* **98** 102504
[28] Bothner D, Gaber T, Kemmler M, Koelle D and Kleiner R 2012 *Phys. Rev. B* **86** 0145517
[29] Song C, DeFeo M P, Yu K and Plourde B L T 2009 *Appl. Phys. Lett.* **95** 232501
[30] Bothner D, Clauss C, Koroknay E, Kemmler M, Gaber T, Jetter M, Scheffler M, Michler P, Dressel M, Koelle D and Kleiner R 2012 *Appl. Phys. Lett.* **100** 012601
[31] Göppl M, Fragner A, Baur M, Bianchetti R, Filipp S, Fink J M, Leek P J, Puebla G, Steffen L and Wallraff A 2008 *J. Appl. Phys.* **104** 113904
[32] Khalil M S, Stoutimore M J A, Wellstood F C and Osborn K D 2012 *J. Appl. Phys.* **111** 054510
[33] Graaf S E, Tzalenchuk A Y and Lindström T 2018 *Appl. Phys. Lett.* **113** 142601